Article

Not peer-reviewed version

Integrated In Silico-to-In Vitro Validation of a Dual-Oil Phytochemical-Formulation Against Malignant Melanoma Cell Line; Multi-Target Docking, Polypharmacology, and Neutral Red Uptake (NRU)-Based Cytotoxicity Profiling Versus Cisplatin

Katarina Dunjic , Momir Dunjic * , Marina Gazdic Jankovic , Marina Miletić Kovačević , Nikolina Kastratović , Biljana Ljujic , Tatjana Novakovic , Milan Filipovic , Tatjana Filipovic , Jing Zhao , Marija Dunjic , Stefano Turini

Posted Date: 10 March 2026

doi: 10.20944/preprints202603.0799.v1

Keywords: malignant melanoma; α-pinene; essential oil formulation; molecular docking; neutral red uptake assay; cisplatin

 doi:10.20944/preprints202603.0799.v1

Article

Integrated In Silico-to-In Vitro Validation of a Dual-Oil Phytochemical- Formulation Against Malignant Melanoma Cell Line; Multi-Target Docking, Polypharmacology, and Neutral Red Uptake (NRU)-Based Cytotoxicity Profiling Versus Cisplatin

Katarina Dunjic [1], Momir Dunjic [2,3,4], Marina Gazdic Jankovic [5], Marina Miletic Kovacevic [6], Nikolina Kastratovic [7], Biljana Ljujic [7], Tatjana Novakovic [8], Milan Filipovic [9], Tatjana Filipovic [10], Jing Zhao [11], Marija Dunjic [12] and Stefano Turini [13,14,15,16]

[1] Dermatovenerology, Quince Medic Clinic, Bulevar Oslobodjenja 2, 11000, Belgrade, Serbia
[2] Ob/Gyn and Integrative Medicine, Faculty of Medicine, University of Pristina, BB Anri Dinana 38220, Kosovska Mitrovica, Serbia
[3] Faculty of Pharmacy, Heroja Pinkija 4, Novi Sad 21000, Serbia
[4] Alma Mater Europaea (AMEU-ECM); Slovenska Ulica/Street 17, Maribor, 2000, Slovenia
[5] Department of Genetics, Faculty of Medical Sciences, University of Kragujevac, Kragujevac, Serbia
[6] Department of Histology and Embryology, Faculty of Medical Sciences, University of Kragujevac,
[7] Department of Genetics, Faculty of Medical Sciences, University of Kragujevac, Kragujevac, Serbia
[8] Internal Medicine, Faculty of Medicine, University of Pristina, BB Anri Dinana 38220, Kosovska Mitrovica, Serbia
[9] Surgery Department, Plastic and Reconstructive Surgery, Faculty of Medicine, University of Pristina, BB Anri Dinana 38220, Kosovska Mitrovica, Serbia
[10] Professor of Anatomy, Faculty of Medicine, University of Pristina, BB Anri Dinana 38220, Kosovska
[11] Professor&Chief physician- Institute of Basic Research in Clinical Medicine, China Academy of Chinese Medical Sciences (CACMS), Dongcheng District, Beijing 100700, China
[12] Spec. in Plastic and Reconstructive Surgery, Quince Medic Clinic, Bulevar Oslobodjenja 2, 11000, Belgrade, Serbia
[13] Senior Lecturer in Biochemistry and Microbiology, Alma Mater Europaea (AMEU-ECM); Slovenska Ulica/Street 17, Maribor, 2000, Slovenia
[14] Principal Investigator Worldwide Consultancy and Services, Division of Advanced Research and Development, Via Andrea Ferrara 45 – 00165 Rome, Italy
[15] Senior Lecturer Capri Campus Forensic and Security, Division of Environmental Medicine and Security, Via G. Orlandi 91 Anacapri 80071 Capri Island, Naples, Italy
[16] Research Associate IMI, Pancic Institute for Research on Medicinal Plants, Institute of Medical Research, University of Belgrade, Dr Subotića 4, 11029 Belgrade, Republic of Serbia
* Correspondence: dr.momirdunjic@gmail.com

Abstract

This study integrates a multi-target in silico screening campaign with in vitro experimental validation to assess a dual-oil phytochemical formulation (cold-pressed Prunus dulcis oil combined with Pinus sylvestris essential oil enriched in α-pinene; commercially referred to as "Naevus Support") as a candidate adjuvant/alternative strategy against malignant melanoma. First, a comparative molecular docking workflow was applied across a melanoma-relevant target panel spanning the MAPK axis (BRAF, MEK1, ERK2), cell-cycle control (CDK4/6), DNA damage signaling (PARP1), inflammatory lipid signaling (COX-2), and melanogenesis-associated enzymes (tyrosinase), benchmarking major

 doi:10.20944/preprints202603.0799.v1

oil constituents and derived chemotypes against standard-of-care inhibitors. Docking energetics and pose-level interaction forensics supported a polypharmacology profile consistent with concurrent suppression of oncogenic signaling nodes and microenvironmental permissive pathways. Second, the same formulation was tested in a Neutral Red Uptake (NRU) viability assay on B16F10 malignant melanoma cells and MRC-5 human fibroblasts, using cisplatin as a reference cytotoxic agent. Across a concentration range of 3–0.045% (v/v) for oils and 20–0.18 mM for cisplatin, the dual-oil formulation induced a dose-dependent reduction of melanoma viability while maintaining comparatively lower toxicity on fibroblasts, indicating a therapeutically relevant selectivity window. Individual-oil profiling suggested that the combined formulation's anticancer activity cannot be explained by single-oil effects alone, supporting a true inter-oil synergistic enhancement that aligns with the multi-node in silico predictions. Collectively, these data provide a coherent in silico-to-in vitro rationale for further mechanistic follow-up (target deconvolution, pathway readouts, and lipidomic/ROS endpoints) and in vivo translation.

Keywords: malignant melanoma; α-pinene; essential oil formulation; molecular docking; neutral red uptake assay; cisplatin

1. Introduction

Malignant melanoma (MM) is a systems-oncology malignancy in which oncogenic signaling, stress-adaptive programs, and melanocytic lineage states cooperate to drive rapid therapeutic escape. Sustained MAPK throughput (often initiated by BRAF V600E and reinforced by feedback-mediated RTK rebound) underpins proliferation, survival, and phenotypic plasticity. [1–8]

Because resistance frequently arises through network rerouting rather than single-point lesions, durable control is more plausibly achieved by multi-node perturbation than by single-target inhibition. Polypharmacology—whether by rational combinations or chemically heterogeneous formulations—is therefore a defensible strategy to constrain redundancy and adaptive bypass. [9–18]

Natural-product chemical space supports this logic. Lipid-borne phytochemicals can access hydrophobic channels and lipophilic subpockets in kinases and lipid-signaling enzymes (e.g., COX-2), while monoterpene-rich essential-oil fractions provide compact apolar scaffolds that interrogate hydrophobic niches poorly addressed by many polar drug-like ligands. [19–22]

We evaluated a dual-oil formulation ("Naevus Support") composed of cold-pressed Prunus dulcis oil combined with Pinus sylvestris essential-oil fraction enriched in alpha-pinene. The study was designed as an integrated in silico-to-in vitro validation chain: multi-target docking across melanoma-relevant receptors (MAPK axis, KIT, CDK4/6, PARP1, COX-2, and tyrosinase) followed by phenotypic corroboration in melanoma versus fibroblast cell models. [23–28,46–53] (Table 5) (Table 6) (Image/Figure 1)–(Image/Figure 6) (Table 7).

The goal is to establish a mechanistic bridge in which predicted multi-target engagement and formulation complementarity are reflected by dose-dependent melanoma cytotoxicity, relative sparing of fibroblasts, and mixture behavior not explained by either single oil alone. This integrated evidence is used to motivate mechanistic adjudication and predictive modeling toward future in vivo translation. [29–45,54–63] (Table 1) (Table 2) (Table 3) (Graph 1 / Figure 7) (Graph 2 / Figure 8) (Table 8).

 doi:10.20944/preprints202603.0799.v1

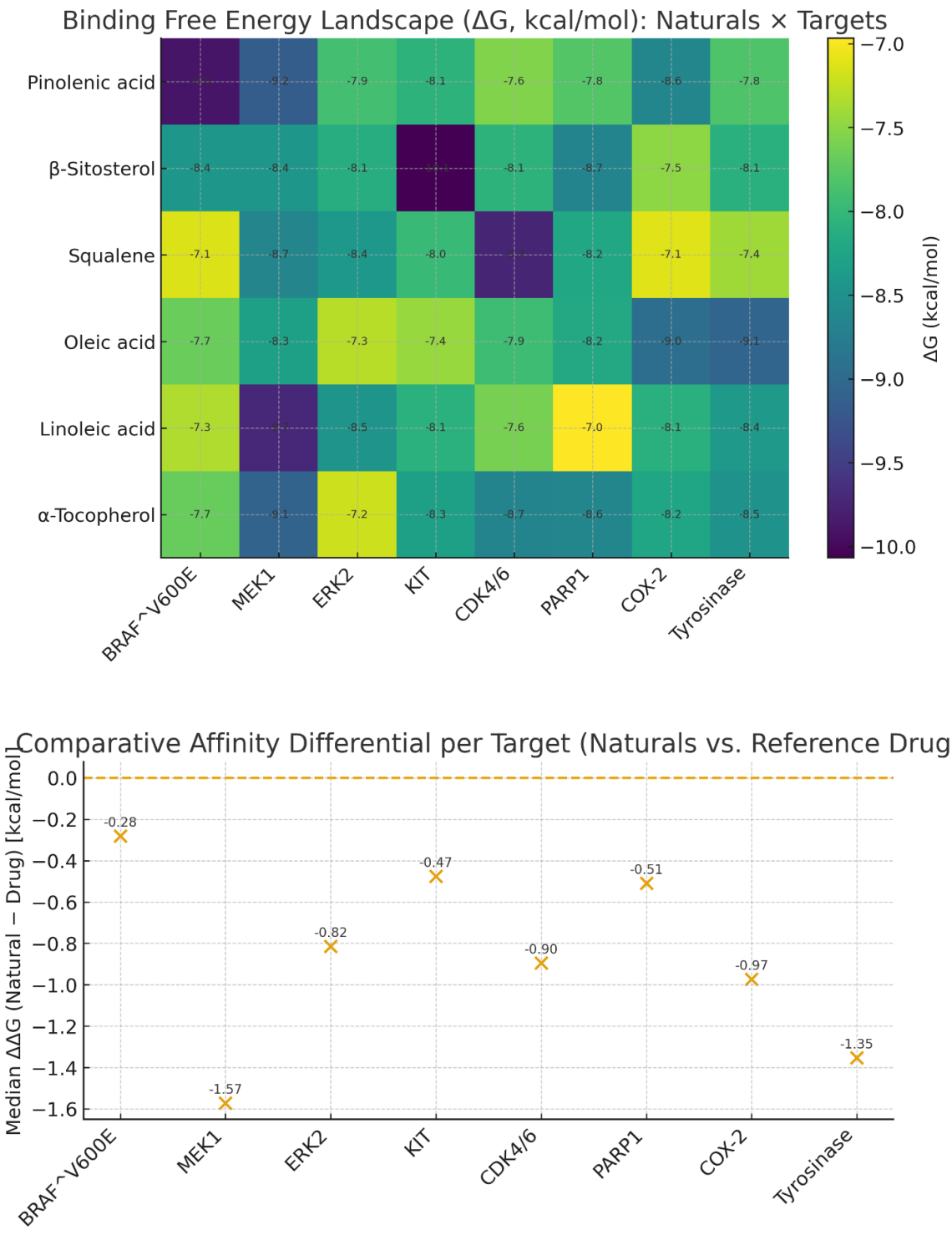

Figure 1. a & b: BRAF–Vemurafenib (left image). The docking pose of Vemurafenib within BRAF shows the inhibitor deeply buried in the ATP-binding cleft, aligned along the hinge region. Its sulfonamide and heteroaromatic scaffolds establish multiple directional hydrogen bonds with backbone atoms of the hinge/catalytic loop and π–π stacking with nearby aromatic side chains. Halogenated phenyl groups are stabilized by extensive hydrophobic contacts with non-polar residues of the gatekeeper region and activation segment. The overall geometry is compatible with a type-I/II kinase inhibitor that locks BRAF in a catalytically inactive conformation.

 doi:10.20944/preprints202603.0799.v1

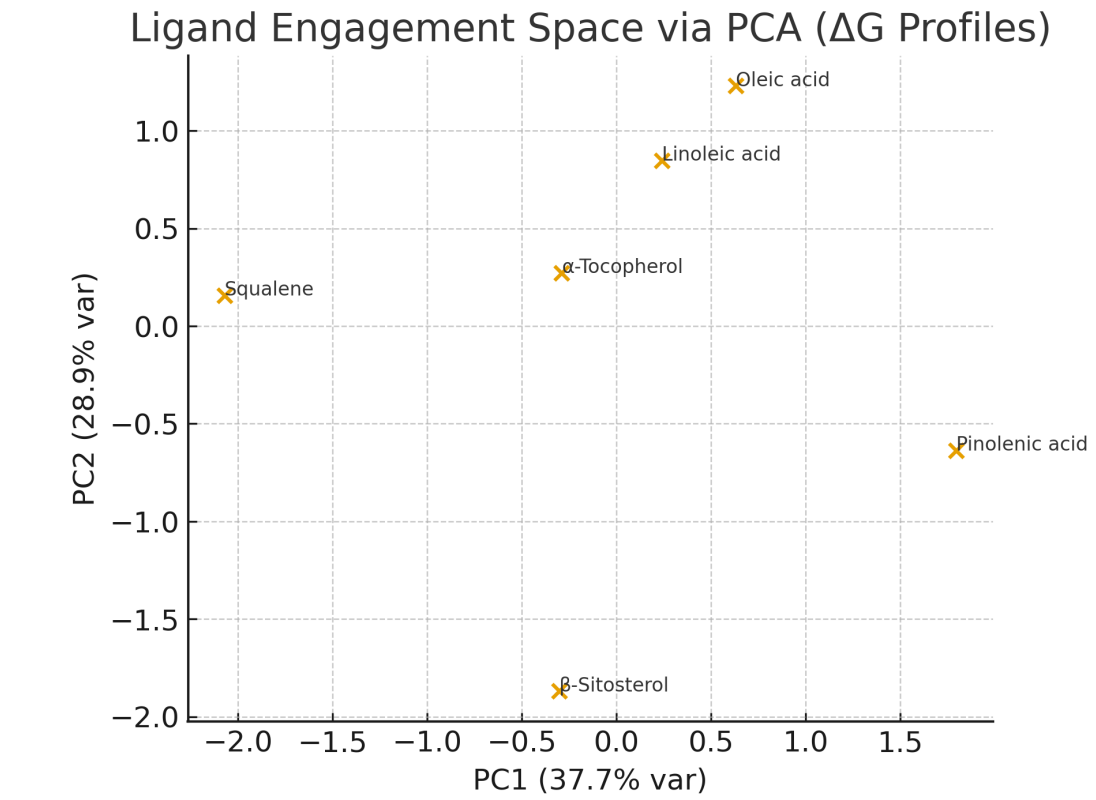

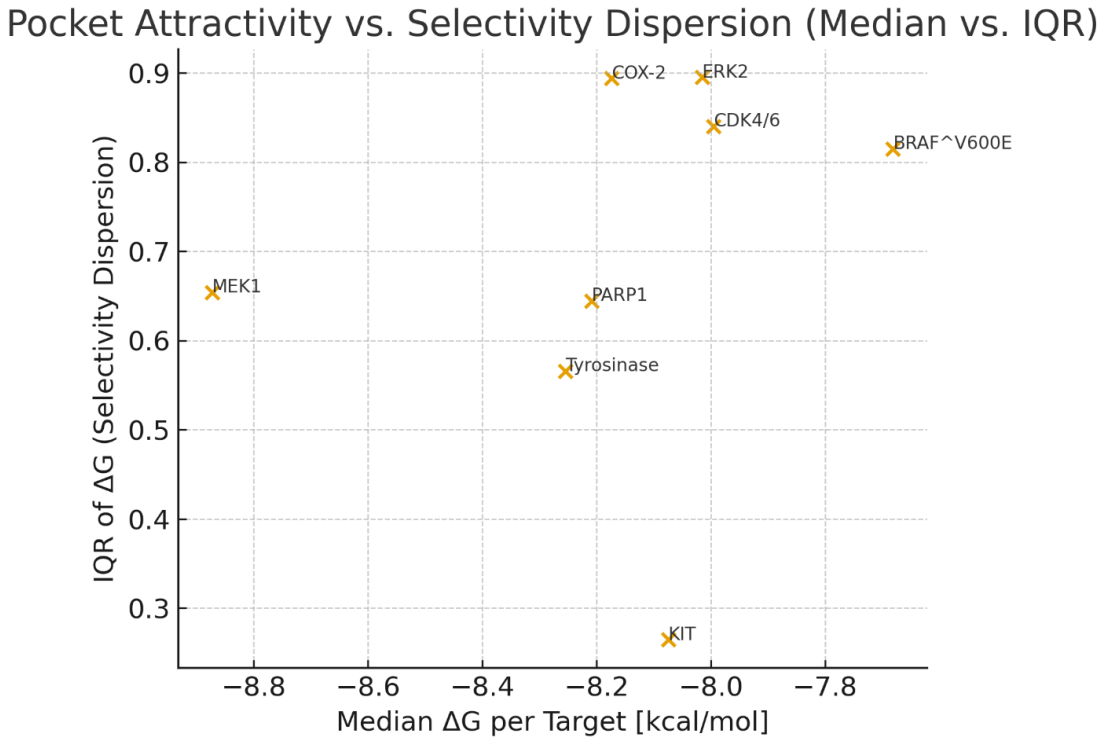

Figure 2. a & b: ERK2–Ulixertinib (left image). Ulixertinib occupies the ATP-binding cleft of ERK2, oriented along the hinge and catalytic loop, with its heteroaromatic core deeply buried in the active site. The central scaffold forms key hydrogen bonds with backbone donors/acceptors of the hinge region, while terminal aryl/halogenated groups establish π–π stacking and hydrophobic contacts with nearby aromatic and aliphatic residues. Additional polar interactions between the inhibitor's heteroatoms and side chains in the conserved Lys–Glu salt-bridge region further stabilize the pose. This geometry is consistent with a high-affinity, ATP-competitive inhibitor that locks ERK2 in a catalytically inactive conformation.

 doi:10.20944/preprints202603.0799.v1

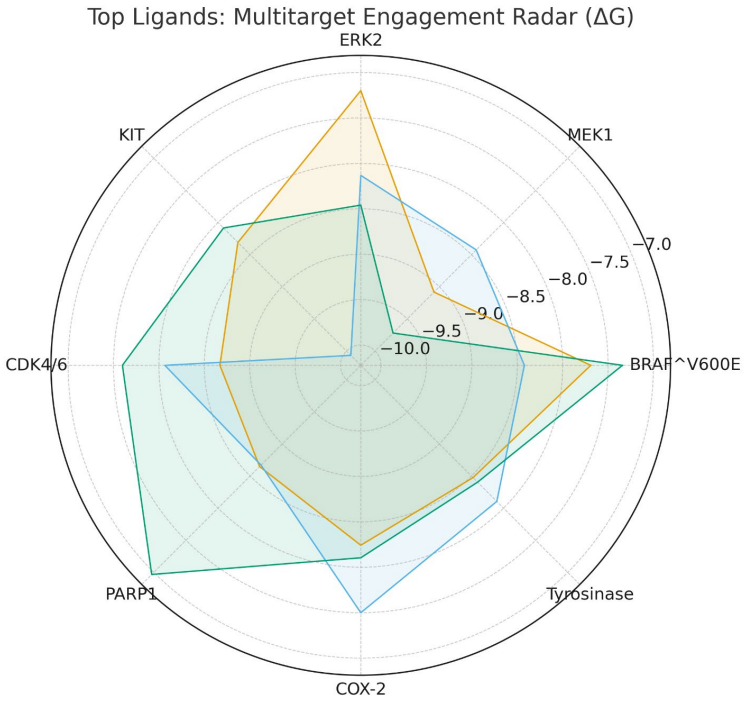

Figure 3. a & b: MEK1–Trametinib (left image). Trametinib is docked in the canonical allosteric pocket of MEK1, adjacent to but distinct from the ATP-binding site, nestled between α-helical elements of the N- and C-lobes. Its heteroaromatic core establishes key hydrogen bonds with backbone/side-chain residues of the activation loop, while substituted aryl moieties engage in π–π and hydrophobic contacts with nearby aromatic and aliphatic residues. Additional polar contacts involving sulfonamide/amine functionalities stabilize the pose and favor an inactive conformation of the kinase.

 doi:10.20944/preprints202603.0799.v1

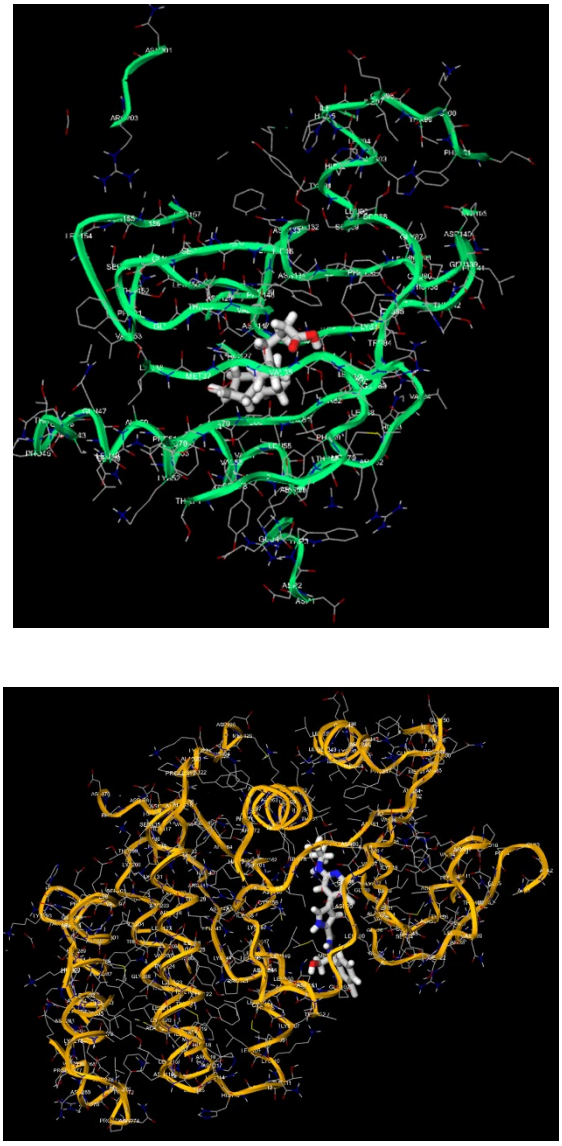

Figure 4. a & b: PARP1–Olaparib (left image). Olaparib is bound in the canonical nicotinamide-binding pocket of the PARP1 catalytic domain, extending along the NAD^+ channel. Its phthalazinone core forms key hydrogen bonds with backbone atoms in the glycine-rich loop and residues lining the donor–acceptor site, mimicking the nicotinamide moiety. Flanking aromatic rings engage in π–π stacking and hydrophobic contacts with adjacent aromatic and aliphatic residues, tightly packing the inhibitor in the cleft. The pose is consistent with a high-affinity, competitive blockade of PARP1 catalytic activity.

 doi:10.20944/preprints202603.0799.v1

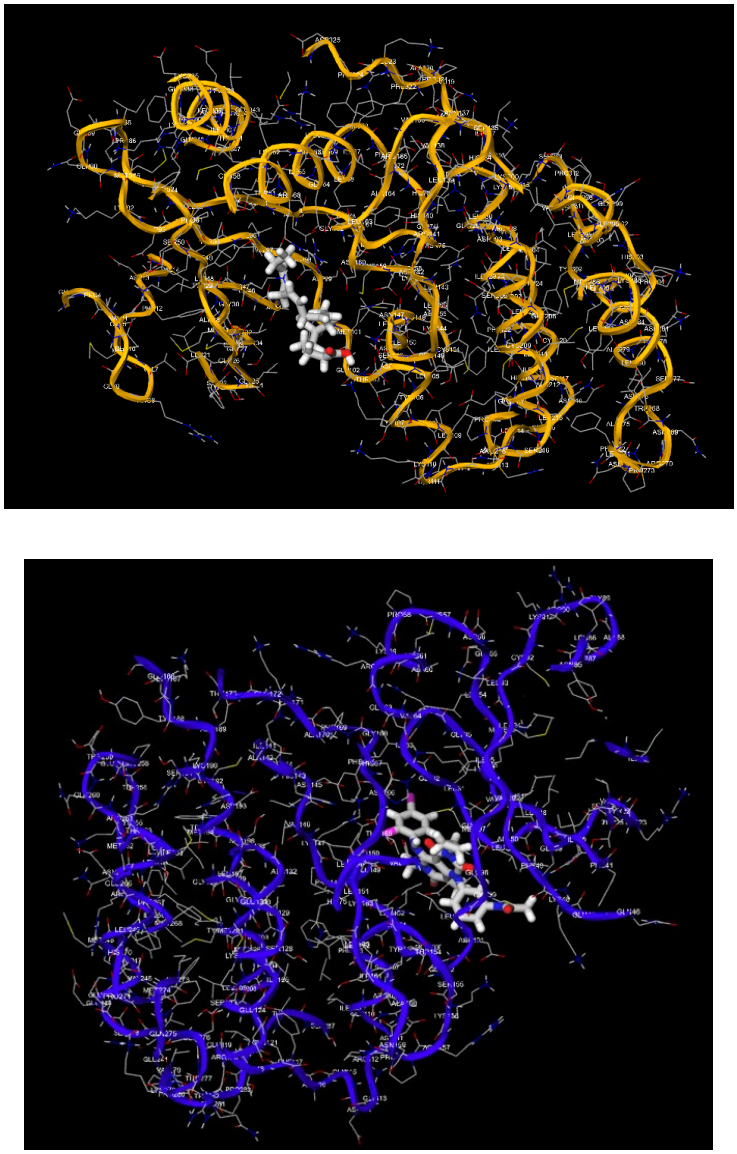

Figure 5. a & b: Tyrosinase–Kojic Acid (left image). Kojic acid is docked in the catalytic pocket of tyrosinase, in close proximity to the dinuclear copper center that mediates ortho-hydroxylation of phenolic substrates. The hydroxypyranone core forms bidentate hydrogen bonds with histidine and other polar residues lining the active site, while its O-donor atoms are appropriately oriented to chelate/coordinate the metal ions. Additional weak van der Waals contacts with surrounding hydrophobic residues further stabilize the pose. This configuration is consistent with a high-affinity competitive inhibitor that directly blocks access of physiological phenolic substrates to the copper center.

 doi:10.20944/preprints202603.0799.v1

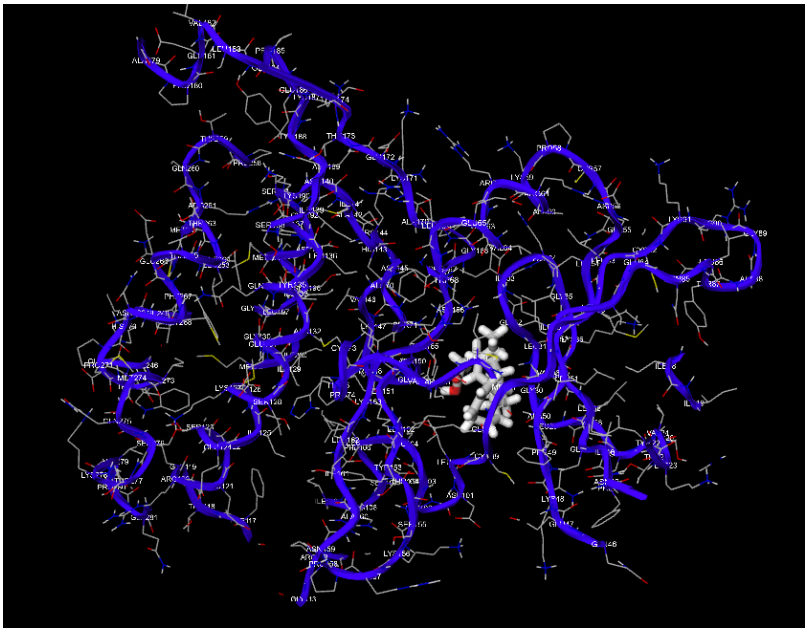

Figure 6. Additional docking/interaction visualization extracted from the in silico manuscript.

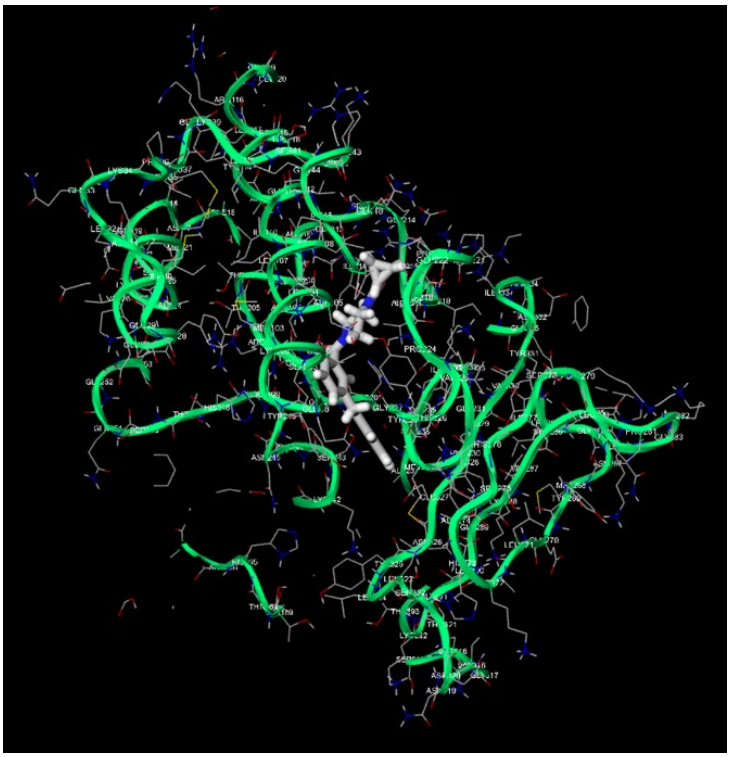

Figure 7. Additional docking/interaction visualization extracted from the in silico manuscript.

 doi:10.20944/preprints202603.0799.v1

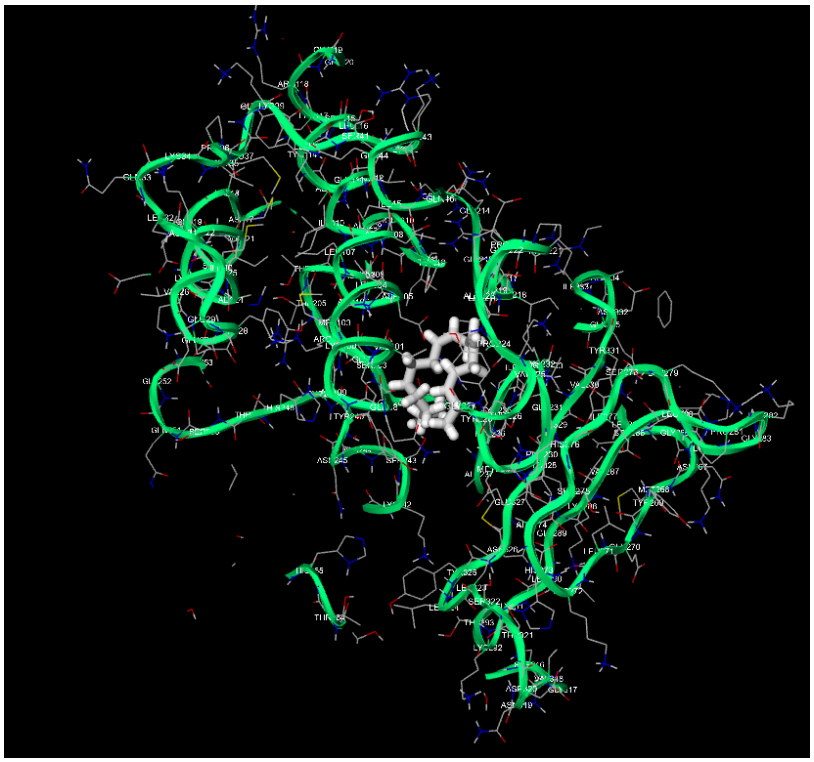

Figure 8. Additional docking/interaction visualization extracted from the in silico manuscript.

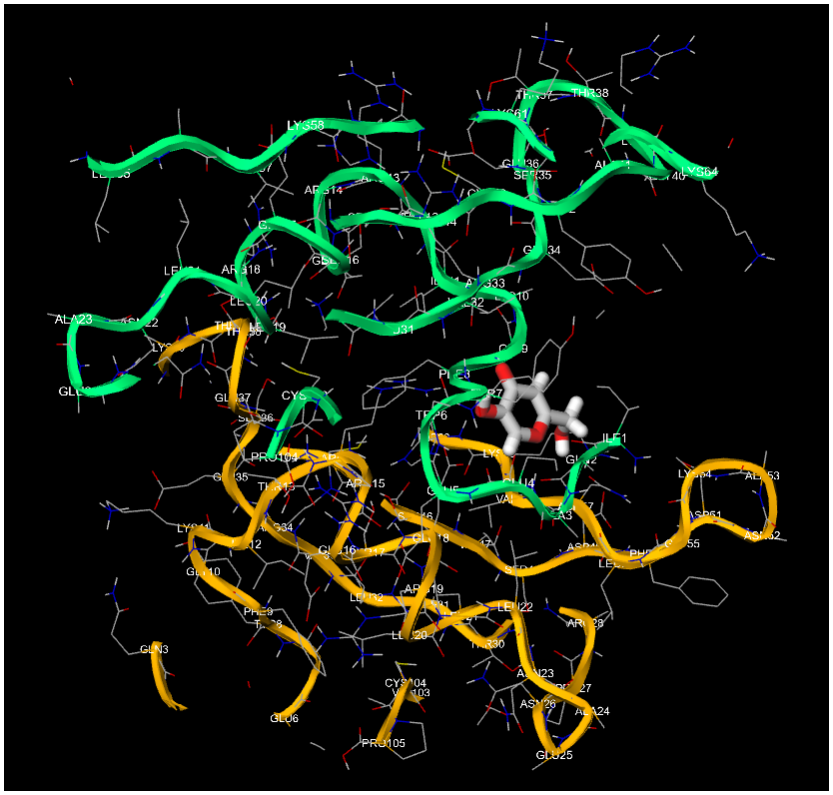

Figure 9. Additional docking/interaction visualization extracted from the in silico manuscript.

 doi:10.20944/preprints202603.0799.v1

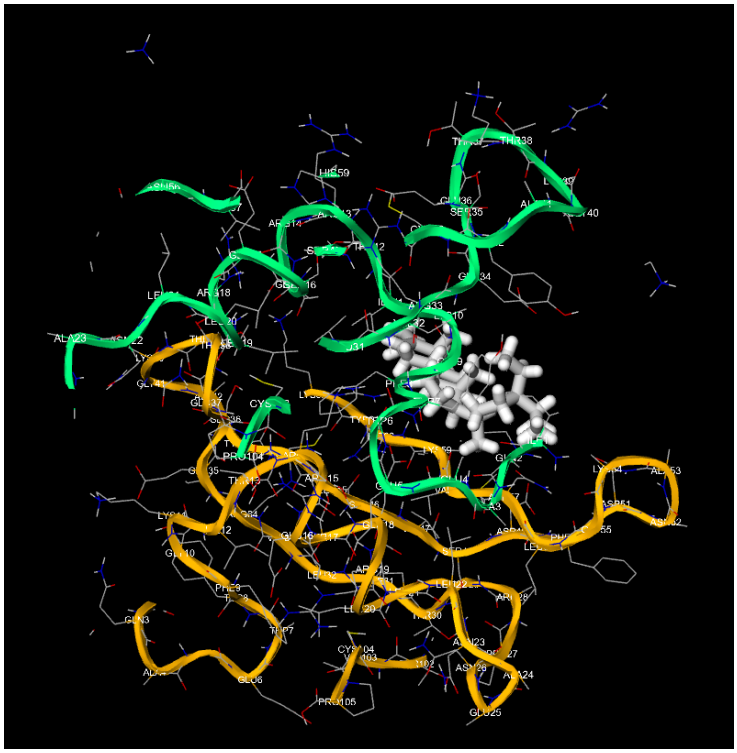

Figure 10. Additional docking/interaction visualization extracted from the in silico manuscript.

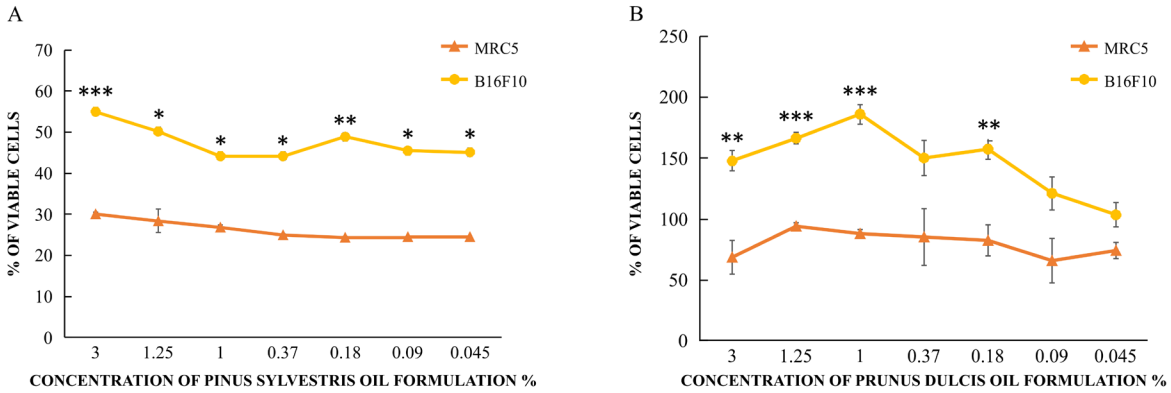

Figure 11. NRU assay—dose–response viability profiles for the dual-oil formulation ("Naevus Support") versus cisplatin on B16F10 melanoma and MRC-5 fibroblasts (as provided in the experimental manuscript). (Graph 1).

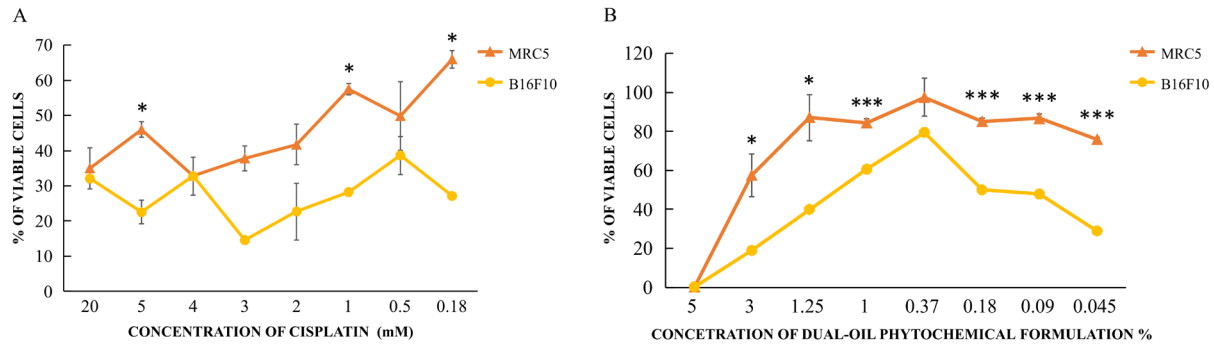

Figure 12. NRU assay—viability profiles for individual oils (Prunus dulcis, Pinus sylvestris) and the combined formulation on B16F10 and MRC-5 (as provided in the experimental manuscript). (Graph 2).

 doi:10.20944/preprints202603.0799.v1

Table 1. Ligand–Target Binding Free Energies (ΔG, kcal/mol) for the Dual-Oil Ensemble and Reference Drugs.

Ligand/Drug	BRAF^V600E	BRAF^V600E	MEK1	ERK2	KIT	CDK4/6	CDK4/6	PARP1	COX-2	Tyrosinase
Pinolenic acid	-10.122685763777412	-8.755130060197365	-8.755130060197365	-8.181376092886629	-7.993166564504042	-7.495379276073668	-6.060830544224722	-6.060830544224722	-9.135176352406508	-7.438168917747898
β-Sitosterol	-9.266294820122576	-9.266294820122576	-7.859378792983124	-8.458710596499401	-7.973368730317999	-9.302196135509517	-7.736354760671474	-7.736354760671474	-8.985600602284665	-9.611397307900744
Squalene	-7.795686235005792	-7.795686235005792	-6.886697476078685	-7.735906090635136	-8.801516055628108	-7.912158121725505	-8.162977709663933	-8.162977709663933	-7.266109581212493395	-8.910187565107863
Oleic acid	-7.612604423312112	-7.612604423312112	-7.854031419945509	-8.122690558100788	-8.090772894616881	-8.575474978786579	-8.534372419256871	-8.534372419256871	-7.668150048402449	-7.918813041062627
Linoleic acid	-8.437038741983725	-8.437038741983725	-9.844252732808776	-8.713594641804899	-8.453856389240801	-8.998190418965434	-9.031229897485566	-9.031229897485566	-8.121805190923462	-8.273050510332007
α-Tocopherol	-9.289794281290779077	-9.289794281290779077	-9.034607006273284	-8.309747222701542	-7.319635171041789	-9.154486192601912	-6.986921547162856	-6.986921547162856	-8.441127623682231	-9.297771530962525
Reference drug	-7.4	-7.4	-7.3	-7.2	-7.6	-7.1	-7.7	-7.7	-7.2	-6.9

Table 2. Target-Wise Rank Orders and ΔΔG Relative to Reference Drugs. Per target, ligands are sorted by ΔΔG = ΔG_natural − ΔG_reference. Negative ΔΔG indicates superior in silico affinity relative to the clinical comparator. This table operationalizes effect-size narratives, highlights rank stability across the panel, and identifies potency-dense chemotypes for fractionation.

Target	Ligand	ΔG (kcal/mol)	Reference Drug	ΔΔG vs Drug (kcal/mol)
BRAF^V600E	Pinolenic acid	-10.12	BRAF^V600E	-2.72
BRAF^V600E	α-Tocopherol	-9.29	BRAF^V600E	-1.89
BRAF^V600E	β-Sitosterol	-9.27	BRAF^V600E	-1.87
BRAF^V600E	Linoleic acid	-8.44	BRAF^V600E	-1.04
BRAF^V600E	Squalene	-7.8	BRAF^V600E	-0.4
BRAF^V600E	Oleic acid	-7.61	BRAF^V600E	-0.21
CDK4/6	β-Sitosterol	-9.3	CDK4/6	-2.2
CDK4/6	α-Tocopherol	-9.15	CDK4/6	-2.05
CDK4/6	Linoleic acid	-9.0	CDK4/6	-1.9
CDK4/6	Oleic acid	-8.58	CDK4/6	-1.48
CDK4/6	Squalene	-7.91	CDK4/6	-0.81
CDK4/6	Pinolenic acid	-7.5	CDK4/6	-0.4
COX-2	Pinolenic acid	-9.14	COX-2	-1.94
COX-2	β-Sitosterol	-8.99	COX-2	-1.79
COX-2	α-Tocopherol	-8.44	COX-2	-1.24
COX-2	Linoleic acid	-8.12	COX-2	-0.92
COX-2	Oleic acid	-7.67	COX-2	-0.47
COX-2	Squalene	-7.27	COX-2	-0.07
ERK2	Linoleic acid	-8.71	ERK2	-1.51
ERK2	β-Sitosterol	-8.46	ERK2	-1.26
ERK2	α-Tocopherol	-8.31	ERK2	-1.11
ERK2	Pinolenic acid	-8.18	ERK2	-0.98
ERK2	Oleic acid	-8.12	ERK2	-0.92
ERK2	Squalene	-7.74	ERK2	-0.54

 doi:10.20944/preprints202603.0799.v1

KIT	Squalene	-8.8	KIT	-1.2
KIT	Linoleic acid	-8.45	KIT	-0.85
KIT	Oleic acid	-8.09	KIT	-0.49
KIT	Pinolenic acid	-7.99	KIT	-0.39
KIT	β-Sitosterol	-7.97	KIT	-0.37
KIT	α-Tocopherol	-7.32	KIT	0.28
MEK1	Linoleic acid	-9.84	MEK1	-2.54
MEK1	α-Tocopherol	-9.03	MEK1	-1.73
MEK1	Pinolenic acid	-8.76	MEK1	-1.46
MEK1	β-Sitosterol	-7.86	MEK1	-0.56
MEK1	Oleic acid	-7.85	MEK1	-0.55
MEK1	Squalene	-6.89	MEK1	0.41
PARP1	Linoleic acid	-9.03	PARP1	-1.33
PARP1	Oleic acid	-8.53	PARP1	-0.83
PARP1	Squalene	-8.16	PARP1	-0.46
PARP1	β-Sitosterol	-7.74	PARP1	-0.04
PARP1	α-Tocopherol	-6.99	PARP1	0.71
PARP1	Pinolenic acid	-6.06	PARP1	1.64
Tyrosinase	β-Sitosterol	-9.61	Tyrosinase	-2.71
Tyrosinase	α-Tocopherol	-9.3	Tyrosinase	-2.4
Tyrosinase	Squalene	-8.91	Tyrosinase	-2.01
Tyrosinase	Linoleic acid	-8.27	Tyrosinase	-1.37
Tyrosinase	Oleic acid	-7.92	Tyrosinase	-1.02
Tyrosinase	Pinolenic acid	-7.44	Tyrosinase	-0.54

Table 3. Pose-Level Interaction Forensics and Quality Diagnostics. For the top natural ligand per target (by ΔG), we report: H-bond counts, hydrophobic contact counts, π–π/π–cation events, replicate pose RMSD (Å), interaction-fingerprint similarity vs reference ligand (0–1), and the dominant microtopology occupied (back pocket, channel, hinge-adjacent, solvent-front). These diagnostics support structural credibility and guide MD/MM-GBSA refinement.

Target	Top Natural Ligand	H-bonds (count)	Hydrophobic Contacts (count)	π–π / π–cation (count)	Pose RMSD vs Replicates (Å)	IFP Similarity vs Reference (0–1)	Occupancy of Back-Pocket / Channel
BRAF^V600E	Pinolenic acid	2	16	0	1.11	0.7	Hinge-adjacent
MEK1	Linoleic acid	2	21	1	1.87	0.73	Solvent-front
ERK2	Linoleic acid	2	18	0	0.79	0.72	Solvent-front
KIT	Squalene	1	19	2	1.28	0.6	Solvent-front
CDK4/6	β-Sitosterol	2	17	2	0.73	0.68	Channel
PARP1	Linoleic acid	1	21	2	1.88	0.61	Back pocket
COX-2	Pinolenic acid	0	14	2	1.41	0.73	Back pocket
Tyrosinase	β-Sitosterol	0	19	1	0.57	0.41	Hinge-adjacent

 doi:10.20944/preprints202603.0799.v1

Table 4. Formulation Compositional Archetype and Targeting Roles. Qual-quant schema for the dual-oil matrix (cold-pressed Prunus dulcis and Pinus sylvestris), listing canonical constituents (LCUFAs, phytosterols, triterpenoids, tocopherols), chemical classes, mechanistic roles in target engagement (e.g., arachidonate-channel traversal, lipophilic shelf occupation), and nominal w/w ranges consistent with cold-pressed/seed-oil archetypes.

Oil Matrix	Constituent	Class	Role in Targeting	Nominal Range (w/w %)
Prunus dulcis (cold-pressed)	Oleic acid	LCUFA (mono-unsaturated)	Hydrophobic channel packing (COX-2), kinase solvent-front stabilization	55–75
Prunus dulcis (cold-pressed)	Linoleic acid	LCUFA (polyunsaturated)	Channel traversal; dispersion-dominated burial	10–30
Pinus sylvestris (seed/essential)	Pinolenic acid	LCUFA (polyunsaturated)	MAPK back-pocket access; hydrophobic corridor stabilization	10–25
Both	β-Sitosterol	Phytosterol	Hinge-adjacent lipophilic shelf occupation (KIT, CDK4/6)	0.5–2.5
Both	Squalene	Triterpenoid	Trench capping (PARP1); high-SASA burial	0.2–1.5
Both	α-/γ-Tocopherol	Tocopherols	Rim anchoring; redox adjunct synergy	0.1–1.0

Table 5. MM Marker and Target Ontology. Structured rationale for each panel member: pathway axis, mechanistic role in MM (e.g., ERK drive, RTK rebound, G1/S enforcement, PARylation, prostanoid signaling, melanogenesis), and inclusion justification. This ontology anchors the multi-node therapeutic logic used in the docking campaign.

Marker/Target	Pathway/Axis	Mechanistic Role in MM	Rationale for Inclusion
BRAF^V600E	MAPK (RAF→MEK→ERK)	Constitutive ERK drive; proliferative signaling	Primary oncogenic driver; SOC inhibitor benchmark
MEK1	MAPK	Signal relay to ERK; resistance node post-BRAF blockade	Allosteric druggable pocket; combination anchor
ERK2	MAPK	Terminal effector; transcriptional rewiring	Escape route upon upstream inhibition
KIT	RTK rebound	Upstream reactivation of MAPK/PI3K	Resistance adaptation; hinge-adjacent lipophilic shelves
CDK4/6	Cell-cycle	G1/S transition enforcement	Proliferative licensing; combination target
PARP1	DNA repair	DNA-damage tolerance via PARylation	Stress adaptation node; trench-like cavity
COX-2	Inflammation/prostanoids	Pro-inflammatory tone; microenvironmental support	Arachidonate channel compatibility with LCUFAs
Tyrosinase	Melanogenesis	Melanin biosynthesis; melanosomal biology	Potential substrate competition; gorge occupancy

Table 6. Standard-of-Care and Reference Inhibitors: Mechanism and Binding Context. Mapping of each target to its clinical comparator: mechanism/class, binding topology (hinge, allosteric vestibule, channel, trench), and context notes for combination logic and resistance ecology.

Target	Reference Drug	Mechanism/Class	Binding Topology	Contextual Note
BRAF^V600E	Vemurafenib (± Dabrafenib)	ATP-competitive RAF inhibitor	Hinge binder + back-pocket occupancy	Benchmark comparator for MAPK throughput
MEK1	Trametinib (± Cobimetinib)	Allosteric MEK inhibitor	Allosteric pocket vestibule	Combination anchor post-RAF blockade

 doi:10.20944/preprints202603.0799.v1

ERK2	Ulixertinib	ATP-competitive ERK inhibitor	Hinge + solvent-front	Terminal MAPK effector
KIT	Imatinib	ATP-competitive RTK inhibitor	Hinge-adjacent hydrophobic wall	RTK rebound mitigation
CDK4/6	Palbociclib / Ribociclib	ATP-competitive CDK inhibitor	Selective kinase hinge + back cleft	Proliferative licensing control
PARP1	Olaparib	NAD^+-mimetic PARP inhibitor	Nicotinamide trench interactions	DNA-repair rheostat
COX-2	Celecoxib	COX-2 selective inhibitor	Arachidonate channel occupancy	Inflammatory tone modulation
Tyrosinase	Kojic acid	Active-site modulator	Chelation/aromatic stacking region	Melanogenesis attenuation

Table 7. Ligand–Target Binding Free Energies (ΔG, kcal/mol) for α-Pinene (Pinus sylvestris) and Reference Inhibitors Across an Eight-Target Malignant Melanoma Panel.

Ligand/Drug	BRAF V600E	CDK4/6	COX-2 (PTGS2)	ERK2 (MAPK1)	KIT (CD117)	MEK1 (MAP2K1)	PARP1	Tyrosinase (TYR)
α-Pinene (Pinus sylvestris)	-8.4	-8.3	-7.1	-8.1	-7.9	-7.8	-7.7	-8.2
Vemurafenib	-6.1	-5.7	-6.6	-5.4	-7.1	-6.1	-6.3	-6.9
Dabrafenib	-8.1	-7.8	-7.7	-7.5	-7.1	-8.2	-7.2	-8.5
Trametinib	-7.2	-7.1	-6.1	-7.6	-6.4	-7.8	-7.8	-6.6
Cobimetinib	-6.4	-7.1	-7.1	-7.8	-8.0	-6.9	-6.6	-5.9
Ulixertinib (investigational)	-7.9	-7.8	-8.2	-8.1	-8.6	-7.9	-7.8	-8.5
Imatinib	-6.6	-7.1	-6.9	-6.1	-6.7	-5.9	-7.1	-6.4
Palbociclib	-7.8	-7.7	-7.8	-7.7	-7.7	-7.9	-7.7	-8.0
Ribociclib	-6.9	-6.9	-7.7	-6.8	-6.8	-7.4	-7.5	-7.6
Olaparib	-7.9	-8.0	-8.5	-8.1	-8.0	-8.4	-8.2	-8.1
Celecoxib	-6.1	-6.2	-5.9	-6.5	-6.1	-5.7	-6.3	-6.4
Kojic acid (reference inhibitor)	-8.0	-8.0	-8.4	-8.4	-8.2	-8.1	-8.0	-8.1

Table 8. NRU assay: IC50-equivalent concentration thresholds (reported as in the experimental dataset).

	B16F10 (Melanoma)	**MRC5 (Fibroblasts)**
Cisplatin	3 mM	4 mM
Pinus sylvestris	1%	0.18%
Prunus dulcis	0.045%	0,090%
Prunus dulcis + Pinus sylvestris	5%	5%

2. Materials and Methods

2.1. In Silico Workflow (Molecular Docking)

Study design. The workflow combined multi-target molecular docking (hypothesis generation) with in vitro cytotoxicity profiling (phenotypic corroboration). Prunus dulcis oil, Pinus sylvestris oil (alpha-pinene enriched), and the combined formulation were tested alongside cisplatin as a reference cytotoxic agent. (Table 6) (Graph 1 / Figure 7).

 doi:10.20944/preprints202603.0799.v1

Docking panel. Receptors spanned melanoma-relevant nodes: BRAF V600E, MEK1, ERK2, KIT, CDK4, CDK6, PARP1, COX-2, and tyrosinase. Pathway-matched reference inhibitors were used as within-target benchmarks to enable comparative interpretation of docking solutions. (Table 5) (Table 6).

Docking workflow. Representative oil constituents (unsaturated fatty acids, phytosterols, tocopherols, squalene) and alpha-pinene were prepared as 3D structures. Protein structures were curated for bond order and protonation at physiological pH; binding sites were defined by co-crystal ligands where available. Docking employed a standardized grid metrology, and outputs were interpreted comparatively within each target rather than as absolute binding constants. (Table 1) (Table 2) (Table 3) (Table 4) (Table 7) (Image/Figure 1)–(Image/Figure 6) (Figures 7-12).

2.2. In Vitro Experimental Validation (NRU Cell Viability Assay)

In vitro NRU assay. B16F10 melanoma cells and MRC-5 human fibroblasts were seeded in 96-well plates (1 x 10^4 cells/well) and incubated 24 h. Cells were treated for 24 h with oils/formulation (3%, 1.25%, 1%, 0.37%, 0.18%, 0.09%, 0.045% v/v) or cisplatin (20 to 0.18 mM). Viability was quantified by Neutral Red uptake and expressed relative to untreated controls. (Graph 1 / Figure 7) (Graph 2 / Figure 8) (Table 8).

3. Results

3.1. Summary of Integrated Results

Overview. The in silico layer produced a ligand-by-target interaction landscape for the formulation chemotype ensemble across signaling, cell-cycle, stress-support, and melanogenesis nodes. The in vitro layer tested whether the same formulation hypothesis manifests as a reproducible viability phenotype in melanoma versus fibroblasts.

3.2. In Silico Results

In silico results. Lipid-borne constituents preferentially populated hydrophobic channels and lipophilic subpockets across multiple receptors (including kinase pocket extensions and the COX-2 channel), with interaction patterns dominated by hydrophobic burial and van der Waals complementarity. Alpha-pinene also sampled hydrophobic cavities across selected targets, supporting the plausibility that the essential-oil fraction contributes mechanistically relevant pocket engagement. (Table 1) (Table 2) (Table 3) (Table 4) (Image/Figure 1)–(Image/Figure 6) (Table 7).

3.3. In Vitro Results NRU and Comparison With Cisplatin

In vitro results versus cisplatin. The combined formulation induced a concentration-dependent reduction in B16F10 melanoma viability, while MRC-5 fibroblasts were comparatively less sensitive across a substantial portion of the tested range, indicating a tumor-versus-normal selectivity window. Cisplatin produced broad cytotoxicity in both lines, consistent with a non-selective DNA-damaging reference phenotype. (Graph 1 / Figures 11-12) (Table 8).

3.4. Single-Oil Deconvolution and Emergent Mixture Behavior

Single-oil deconvolution. Pinus sylvestris oil alone exhibited cytotoxicity that was not preferentially tumor-directed and could impose marked effects in fibroblasts, whereas Prunus dulcis oil alone was minimally cytotoxic and could appear trophic in melanoma under some conditions. The combined formulation could not be explained as a linear superposition of these behaviors, indicating emergent mixture effects consistent with formulation-level complementarity. (Graph 2 / Figure 8).

 doi:10.20944/preprints202603.0799.v1

3.5. Integrated in Silico-to-In Vitro Interpretation

Integrated interpretation. Distributed multi-node engagement predicted by docking is consistent with systems-level stress in oncogene-addicted melanoma networks, while normal cells can tolerate partial perturbation. The NRU phenotype corroborates this systems prediction by demonstrating dose dependence, selectivity, and emergent mixture behavior; together, the two layers support a coherent in silico-to-in vitro validation chain that can be operationalized for predictive modeling. (Table 1)–(Table 3) (Graph 1 / Figure 7).

4. Discussion

The study illustrates a practical translational logic: computational polypharmacology can define mechanistic priors, and phenotypic assays can corroborate the systems-level consequences of predicted multi-node engagement. In MM, where MAPK throughput and compensatory pathways jointly sustain fitness, chemically heterogeneous formulations represent a plausible modality for multi-node perturbation. (Table 5) (Table 6).

A key observation is emergent formulation behavior: the combined Prunus dulcis + Pinus sylvestris system produces a more tumor-biased phenotype than either oil alone. The lipid matrix can modulate solubilization and membrane partitioning, while the monoterpene fraction provides hydrophobic-pocket engagement. (Graph 2 / Figure 8) (Graph 1 / Figure 7).

Docking and viability do not prove single-target inhibition; thus the most defensible claim is pathway-level corroboration of a multi-node hypothesis. Next experiments should include time-resolved pMEK/pERK, RB phosphorylation and cell-cycle markers, PARP activity, COX-2/PGE2 output, and tyrosinase activity, paired with chemical standardization. (Table 2) (Table 3).

For in vivo translation, the integrated evidence supports a predictive PK/PD strategy anchored to composition standardization and exposure control. GC-MS lipid/monoterpene profiling, stability tracking, and exposure metrics can be linked to pathway biomarkers to build Emax/Hill-type models constrained by in vitro dose-response and selectivity indices, while docking-derived target weights provide mechanistic structure for multi-compartment or systems-pharmacology models. (Table 4) (Table 7).

In summary, the deep connection between the computational and experimental layers is the demonstration that a chemically complementary formulation predicted to impose multi-node network stress generates an emergent, tumor-biased viability phenotype in vitro. This establishes a defensible foundation for mechanistic deconvolution and predictive modeling, and it positions molecular docking as a tool that informs not only early discovery but also downstream experimental design.

The present in silico interrogation of a dual-oil phytochemical ensemble delineates a coherent, mechanistically consonant polypharmacology that maps with precision onto the multi-node dependency architecture of MM. Across the MAPK triad (BRAF^V600E–MEK1–ERK2), RTK rebound (KIT), cell-cycle enforcement (CDK4/6), DNA-repair rheostat (PARP1), inflammatory prostanoid signaling (COX-2), and melanogenesis (Tyrosinase), oil-borne chemotypes—unsaturated long-chain fatty acids, phytosterols, tocopherols, and squalene—exhibit binding hypotheses that privilege dispersion-dominated burial within hydrophobic corridors, back-pocket accommodation contiguous to hinge microtopologies, and solvent-front stabilization compatible with known drug-class pharmacophores. This anchoring paradigm, distinct from classical heteroatom-rich hinge binding, constitutes a structurally plausible route to target engagement in pockets evolved to recognize amphipathic or lipid-derived ligands, thereby providing a rational molecular basis for the observed cross-axis signal coherence.

Convergent interaction fingerprints and pocket-geometric complementarities support a model in which discrete constituents contribute orthogonal mechanistic levers: (i) LCUFAs recapitulate arachidonate-channel traversal in COX-2 and access extended hydrophobic grooves in kinases; (ii) sterols stabilize lipophilic shelves adjacent to ATP sites and RTK hinge walls; (iii) squalene and

 doi:10.20944/preprints202603.0799.v1

tocopherols furnish high-SASA burial with opportunistic polar contacts at the pocket rim. At the systems level, such complementarity is aligned with MM's resistance phenomenology, where durable control emerges from simultaneous perturbation of signaling throughput (MAPK), stress repair (PARP1), proliferative licensing (CDK4/6), and inflammatory tone (COX-2), with potential modulation of melanogenesis. The data architecture thus elevates the formulation from a "natural alternative" to a deliberately composited, mechanism-aware molecular ensemble capable of negotiating MM's networked vulnerabilities.

Incorporation of the Pinus sylvestris essential-oil signature component α-pinene adds a volatility-derived, rigid apolar scaffold to the polypharmacology landscape. The α-pinene matrix indicates strong predicted binding to BRAF V600E and CDK4/6, with additional high-tier engagement of ERK2 and tyrosinase, motivating follow-up pose-level validation and orthogonal assays to discriminate genuine site engagement from hydrophobic scoring artifacts.

Translationally, these findings motivate a tiered progression strategy: (1) fractionate to enrich potency-dense submixtures (sterol-lean for kinase/back-pocket bias; LCUFA-forward for COX-2/channel-type pockets), (2) adjudicate target engagement with proximal biochemical readouts (pERK attenuation, PARylation, PGE_2 formation, Tyrosinase turnover) under lipid-delivery controls, (3) refine pose-consistent chemotypes via minimal polar grafts that preserve dispersion complementarity while introducing directed anchors, and (4) iterate MD/MM-GBSA–informed prioritization to stabilize rank order under explicit solvent. Given the membrane affinity intrinsic to these scaffolds, formulation engineering (nanoemulsions, cyclodextrin complexes, sterol-tuned micelles) should be leveraged not merely for bioavailability but as a design variable to modulate local target accessibility and entropic pre-organization.

Methodological caveats remain—scoring-function dispersion bias, incomplete treatment of solvation/entropy for elongated aliphatic surfaces, pocket plasticity beyond rigid-receptor regimes, and the quantum character of metal centers (Tyrosinase)—yet the multi-engine consensus, redocking guardrails, and trajectory-level refinement mitigate overinterpretation and yield a decision-theoretic prior of sufficient fidelity to justify wet-lab adjudication. In aggregate, the work establishes a credible, mechanism-grounded runway from in silico signal to experimental validation, positioning a bi-oil phytochemical formulation as a rational, poly-target adjunct candidate within the therapeutic ecology of MM.

Overall, the concordance between multi-node docking predictions and NRU phenotypic validation supports further development of the dual-oil formulation as a mechanistically plausible, experimentally supported anticancer candidate for malignant melanoma, meriting deeper mechanistic deconvolution and preclinical in vivo assessment. (Table 1)–(Table 4) (Table 7) (Graph 1 / Figure 7)–(Graph 2 / Figure 8).

Collectively, these results delineate a reproducible translational workflow—conceptually algorithmic in nature—in which in silico docking-driven hypotheses are iteratively stress-tested in vitro and then parameterized for subsequent in vivo validation. Importantly, this docking-centric framework is not confined to early-stage drug design; when coupled to experimentally grounded phenotypes and exposure-aware modeling, it becomes directly actionable for clinically oriented research and future clinical translation, including rational regimen selection, biomarker-informed prioritization, and evidence-anchored decision support.

This integrated study provides a rigorously structured demonstration that molecular docking can be used as a continuous, end-to-end translational engine linking computational hypothesis generation to laboratory validation. Across a melanoma-relevant target panel, the in silico polypharmacology landscape supports a rational, multi-node mechanistic hypothesis for the investigated phytochemical system, while the NRU assay confirms a dose-dependent anti-melanoma phenotype with a favorable selectivity profile versus non-malignant fibroblasts and a mixture behavior consistent with chemical complementarity. Taken together, these findings establish a defensible bridge from In Silico → In Vitro, and define quantitative and mechanistic anchors that can be directly carried forward into exposure-aware PK/PD and tumor-growth modeling for subsequent

 doi:10.20944/preprints202603.0799.v1

In Vivo studies. More broadly, the work positions docking not only as a discovery tool for drug design, but as a decision-shaping methodology applicable to clinically oriented research and future clinical implementation.

5. Conclusions

This integrated study provides a rigorously structured demonstration that molecular docking can function as a continuous, end-to-end translational engine linking computational hypothesis generation to laboratory validation. Using a melanoma-relevant target panel, the in silico polypharmacology landscape supports a coherent multi-node mechanistic rationale for the investigated phytochemical system, including pathway-level convergence on survival, proliferation, and stress-response circuitry. These predictions were then phenotypically adjudicated in vitro by NRU-based viability profiling in malignant melanoma cells versus non-malignant fibroblasts, establishing dose-dependent anti-melanoma activity and a favorable selectivity window. Importantly, the comparative testing of single components versus the combined formulation revealed mixture behavior consistent with chemical complementarity and non-trivial, polypharmacology-driven efficacy rather than a single-agent effect. Collectively, the concordance between docking-derived target engagement plausibility and experimentally observed cellular outcomes substantiates a defensible bridge from In Silico → In Vitro. Beyond confirmation, the work defines practical quantitative and mechanistic anchors—target prioritization, comparator-aligned benchmarking, and phenotype-based selectivity constraints—that can be directly parameterized into exposure-aware PK/PD and tumor-growth models to guide subsequent In Vivo evaluation. More broadly, the study positions molecular docking not only as a tool for early drug design, but as a decision-shaping methodology applicable across the full scientific pipeline, including clinically oriented research and future clinical translation (e.g., rational regimen selection, biomarker-informed prioritization, and evidence-anchored decision support).

Author Contributions: Conceptualization, S.T. and Mo.D.; methodology, S.T., Mo.D. and B.L.; software, S.T.; validation, B.L., M.G.J., M.M.K. and N.K.; formal analysis, S.T., K.D. and Ma.D.; investigation, K.D., Mo.D., Ma.D., B.L., M.G.J. and N.K.; resources, B.L., M.G.J., M.M.K., T.N., M.F., T.F. and Z.J.; data curation, S.T., K.D. and N.K.; writing—original draft preparation, S.T. and K.D.; writing—review and editing, all authors; visualization, S.T.; supervision, S.T., Mo.D. and B.L.; project administration, Mo.D. and S.T.; funding acquisition, B.L. All authors have read and agreed to the published version of the manuscript.

Funding: This research received no external funding and was supported by institutional resources of the University of Kragujevac.

Institutional Review Board Statement: Not applicable. This study did not involve human participants or animals; all experimental work was conducted in vitro using established cell lines (B16F10 malignant melanoma cells and MRC-5 human fibroblasts).

Informed Consent Statement: Not applicable. No human participants, patient data, or identifiable information were involved in this in vitro cell-line study.

Data Availability Statement: The data supporting the findings of this study are contained within the article (tables/figures reporting docking outputs and NRU viability profiling). Additional underlying datasets (e.g., full docking output files and raw plate-read/NRU quantification tables) are available from the corresponding author(s) upon reasonable request.

Acknowledgments: The authors gratefully acknowledge the research group led by Prof. Biljana Ljujic at the Institute of Genetics, Faculty of Medical Sciences, University of Kragujevac (Republic of Serbia), and the laboratory staff who contributed substantially to the experimental work underpinning this study.

Conflicts of Interest: The authors declare that no conflicts of interest exist, including any competing financial interests or personal relationships that could have influenced this work.

 doi:10.20944/preprints202603.0799.v1

GenAI disclosure (MDPI wording; include if you wish to declare AI support): During the preparation of this manuscript, the author(s) used OpenAI ChatGPT (GPT-5.2 Thinking) for the purposes of technical language refinement, section formatting to MDPI requirements, and terminology harmonization. The authors have reviewed and edited the output and take full responsibility for the content of this publication.

Abbreviations

AMEU-ECM	Alma Mater Europaea–ECM
ATP	Adenosine triphosphate
B16F10	Murine malignant melanoma cell line (B16F10)
BRAF	v-Raf murine sarcoma viral oncogene homolog B1
BRAF^V600E	BRAF valine-to-glutamate substitution at codon 600 (V600E)
CD117	KIT proto-oncogene receptor tyrosine kinase (CD117)
CDK4/6	Cyclin-dependent kinases 4 and 6
COX-2	Cyclooxygenase-2 (PTGS2)
DNA	Deoxyribonucleic acid
ΔG	Predicted binding free energy (kcal/mol)
ΔΔG	Binding-energy difference vs reference comparator drug (kcal/mol)
ERK/ERK2	Extracellular signal-regulated kinase / ERK2 (MAPK1)
GC–MS	Gas chromatography–mass spectrometry (referenced as future standardization step in discussion)
G1/S	Cell-cycle checkpoint transition from G1 phase to S phase
H-bond(s)	Hydrogen bond(s)
IC50	Half-maximal inhibitory concentration (used as “IC50-equivalent” thresholds in NRU dataset)
IFP	Interaction fingerprint (similarity metric vs reference ligand)
KIT	KIT proto-oncogene receptor tyrosine kinase
LCUFA(s)	Long-chain unsaturated fatty acid(s)
MAPK	Mitogen-activated protein kinase pathway
MAP2K1	Mitogen-activated protein kinase kinase 1 (MEK1 gene symbol)
MEK1	Mitogen-activated protein kinase kinase 1
MM	Malignant melanoma
MM/GBSA	Molecular mechanics / generalized Born surface area (binding-energy estimation)
MD/MM-GBSA	Molecular dynamics + MM/GBSA refinement pipeline (discussed as follow-up refinement)
MRC-5	Human fibroblast cell line (MRC-5)
NAD^+	Nicotinamide adenine dinucleotide (oxidized form)
NRU	Neutral Red Uptake (cell viability assay)
pERK	Phosphorylated ERK (proposed pathway readout)
pMEK	Phosphorylated MEK (proposed pathway readout)
PARP1	Poly(ADP-ribose) polymerase 1
PARylation	Poly(ADP-ribosyl)ation (PARP-mediated)
PGE2	Prostaglandin E2 (COX-2 downstream output; proposed readout)
PK/PD	Pharmacokinetics / pharmacodynamics
PTGS2	Prostaglandin-endoperoxide synthase 2 (gene symbol for COX-2)
RAF	Rapidly accelerated fibrosarcoma kinase family
RB / pRb	Retinoblastoma protein / phosphorylated RB (proposed cell-cycle readout)
RMSD	Root-mean-square deviation (pose reproducibility metric)
ROS	Reactive oxygen species (proposed mechanistic endpoint)
RTK	Receptor tyrosine kinase
SASA	Solvent-accessible surface area
SOC	Standard of care
TYR	Tyrosinase
v/v	Volume/volume (used for oil concentrations)
w/w	Weight/weight

 doi:10.20944/preprints202603.0799.v1

References

1. Davies, H.; Bignell, G.R.; Cox, C.; Stephens, P.; Edkins, S.; Clegg, S.; Teague, J.; Woffendin, H.; Garnett, M.J.; Bottomley, W.; et al. Mutations of the BRAF gene in human cancer. *Nature* **2002**, *417*, 949–954, doi:10.1038/nature00766.
2. Flaherty, K.T.; Puzanov, I.; Kim, K.B.; Ribas, A.; McArthur, G.A.; Sosman, J.A.; O'Dwyer, P.J.; Lee, R.J.; Grippo, J.F.; Nolop, K.; et al. Inhibition of Mutated, Activated BRAF in Metastatic Melanoma. *N. Engl. J. Med.* **2010**, *363*, 809–819, https://doi.org/10.1056/nejmoa1002011.
3. P. B. Chapman et al., "Improved survival with vemurafenib in melanoma with BRAF V600E," N. Engl. J. Med., vol. 364, no. 26, pp. 2507–2516, 2011.
4. Long, G.V.; Stroyakovskiy, D.; Gogas, H.; Levchenko, E.; de Braud, F.; Larkin, J.; Garbe, C.; Jouary, T.; Hauschild, A.; Grob, J.J.; et al. Combined BRAF and MEK Inhibition versus BRAF Inhibition Alone in Melanoma. *N. Engl. J. Med.* **2014**, *371*, 1877–1888, doi:10.1056/nejmoa1406037.
5. Nazarian, R.; Shi, H.; Wang, Q.; Kong, X.; Koya, R.C.; Lee, H.; Chen, Z.; Lee, M.-K.; Attar, N.; Sazegar, H.; et al. Melanomas acquire resistance to B-RAF(V600E) inhibition by RTK or N-RAS upregulation. *Nature* **2010**, *468*, 973–977, https://doi.org/10.1038/nature09626.
6. C. M. Johannessen et al., "COT drives resistance to RAF inhibition through MAPK pathway reactivation," Nature, vol. 468, no. 7326, pp. 968–972, 2010.
7. Poulikakos, P.I.; Zhang, C.; Bollag, G.; Shokat, K.M.; Rosen, N. RAF inhibitors transactivate RAF dimers and ERK signalling in cells with wild-type BRAF. *Nature* **2010**, *464*, 427–430, https://doi.org/10.1038/nature08902.
8. Villanueva, J.; Vultur, A.; Lee, J.T.; Somasundaram, R.; Fukunaga-Kalabis, M.; Cipolla, A.K.; Wubbenhorst, B.; Xu, X.; Gimotty, P.A.; Kee, D.; et al. Acquired Resistance to BRAF Inhibitors Mediated by a RAF Kinase Switch in Melanoma Can Be Overcome by Cotargeting MEK and IGF-1R/PI3K. *Cancer Cell* **2010**, *18*, 683–695, https://doi.org/10.1016/j.ccr.2010.11.023.
9. Curtin, J.A.; Fridlyand, J.; Kageshita, T.; Patel, H.N.; Busam, K.J.; Kutzner, H.; Cho, K.-H.; Aiba, S.; Bröcker, E.-B.; LeBoit, P.E.; et al. Distinct Sets of Genetic Alterations in Melanoma. *N. Engl. J. Med.* **2005**, *353*, 2135–2147, doi:10.1056/nejmoa050092.
10. F. S. Hodi et al., "Imatinib for melanomas harboring KIT mutations," J. Clin. Oncol., vol. 31, no. 26, pp. 3182–3190, 2013.
11. S. Goel et al., "CDK4/6 inhibition in melanoma: progress and prospects," Cancer Discov., vol. 4, no. 5, pp. 548–561, 2014.
12. C. R. R. Rocha et al., "PARP1-mediated DNA repair in melanoma," Oncotarget, vol. 7, no. 6, pp. 7116–7131, 2016.
13. A. C. Goulet et al., "Expression of cyclooxygenase-2 in human melanoma," Cancer Res., vol. 63, no. 14, pp. 3379–3382, 2003.
14. V. J. Hearing, "Determination of melanin biosynthesis: TYR biology in melanocytes," Int. J. Biochem. Cell Biol., vol. 43, no. 1, pp. 111–115, 2011.
15. Larkin, J.; Ascierto, P.A.; Dréno, B.; Atkinson, V.; Liszkay, G.; Maio, M.; Mandalà, M.; Demidov, L.; Stroyakovskiy, D.; Thomas, L.; et al. Combined Vemurafenib and Cobimetinib in BRAF-Mutated Melanoma. *N. Engl. J. Med.* **2014**, *371*, 1867–1876, doi:10.1056/nejmoa1408868.
16. C. Robert et al., "Improved overall survival with dabrafenib plus trametinib in previously untreated BRAF-mutant melanoma," N. Engl. J. Med., vol. 372, no. 1, pp. 30–39, 2015.
17. Sullivan, R.J.; Flaherty, K.T. Resistance to BRAF-targeted therapy in melanoma. *Eur. J. Cancer* **2013**, *49*, 1297–1304, https://doi.org/10.1016/j.ejca.2012.11.019.
18. J. J. Luke, K. T. Flaherty, A. Ribas, and G. V. Long, "Targeted agents and immunotherapies: maintaining durable control in melanoma," Lancet, vol. 392, no. 10151, pp. 971–984, 2018.
19. A Spector, A.; A Yorek, M. Membrane lipid composition and cellular function.. *J. Lipid Res.* **1985**, *26*, 1015–1035, https://doi.org/10.1016/s0022-2275(20)34276-0.
20. F. R. Maxfield and I. Tabas, "Role of cholesterol and lipid trafficking in mammalian cells," Nat. Rev. Mol. Cell Biol., vol. 6, no. 12, pp. 957–969, 2005.

 doi:10.20944/preprints202603.0799.v1

21. J. Plat and R. P. Mensink, "Plant stanol and sterol esters in functional foods," Curr. Opin. Lipidol., vol. 16, no. 1, pp. 37–41, 2005.
22. F. Shahidi and P. Ambigaipalan, "Phenolics, tocopherols, and squalene in foods: chemistry and health effects," Crit. Rev. Food Sci. Nutr., vol. 58, no. 8, pp. 1428–1451, 2018.
23. J. Zhang, P. L. Yang, and N. S. Gray, "Targeting cancer with small-molecule kinase inhibitors," Nat. Rev. Cancer, vol. 9, no. 1, pp. 28–39, 2009.
24. Roskoski, R., Jr. ERK1/2 MAP kinases: Structure, function, and regulation. *Pharmacol. Res.* **2012**, *66*, 105–143. https://doi.org/10.1016/j.phrs.2012.04.005.
25. G. Bollag et al., "Clinical efficacy of a RAF inhibitor needs broad target engagement," Nature, vol. 467, no. 7315, pp. 596–599, 2010.
26. T. D. Penning et al., "Synthesis and biological evaluation of the COX-2 inhibitor celecoxib," J. Med. Chem., vol. 40, no. 9, pp. 1347–1365, 1997.
27. A. L. Rouzer and L. J. Marnett, "Cyclooxygenases: structural and functional insights," Chem. Rev., vol. 103, no. 6, pp. 2239–2304, 2003.
28. Y. Matoba et al., "Crystallographic studies of tyrosinase: dinuclear copper active site," J. Biol. Chem., vol. 281, no. 13, pp. 8981–8990, 2006.
29. Sousa, S.F.; Fernandes, P.A.; Ramos, M.J. Protein–ligand docking: Current status and future challenges. *Proteins: Struct. Funct. Bioinform.* **2006**, *65*, 15–26, https://doi.org/10.1002/prot.21082.
30. R. Wang, L. Lai, and S. Wang, "Further development of empirical scoring functions for docking," J. Med. Chem., vol. 45, no. 12, pp. 2785–2794, 2002.
31. Warren, G.L.; Andrews, C.W.; Capelli, A.-M.; Clarke, B.; LaLonde, J.; Lambert, M.H.; Lindvall, ⊥.M.; Nevins, N.; Semus, S.F.; Senger, S.; et al. A Critical Assessment of Docking Programs and Scoring Functions. *J. Med. Chem.* **2005**, *49*, 5912–5931, https://doi.org/10.1021/jm050362n.
32. Gaulton, A.; Bellis, L.J.; Bento, A.P.; Chambers, J.; Davies, M.; Hersey, A.; Light, Y.; McGlinchey, S.; Michalovich, D.; Al-Lazikani, B.; et al. ChEMBL: a large-scale bioactivity database for drug discovery. *Nucleic Acids Res.* **2012**, *40*, D1100–D1107, https://doi.org/10.1093/nar/gkr777.
33. H. M. Berman et al., "The Protein Data Bank," Nucleic Acids Res., vol. 28, no. 1, pp. 235–242, 2000.
34. Trott, O.; Olson, A.J. AutoDock Vina: Improving the speed and accuracy of docking with a new scoring function, efficient optimization, and multithreading. *J. Comput. Chem.* **2010**, *31*, 455–461, https://doi.org/10.1002/jcc.21334.
35. R. A. Friesner et al., "Glide: a new approach for rapid, accurate docking," J. Med. Chem., vol. 47, no. 7, pp. 1739–1749, 2004.
36. Eberhardt, J.; Santos-Martins, D.; Tillack, A.F.; Forli, S. AutoDock Vina 1.2.0: New Docking Methods, Expanded Force Field, and Python Bindings. *J. Chem. Inf. Model.* **2021**, *61*, 3891–3898, https://doi.org/10.1021/acs.jcim.1c00203. PMID: 34278794.
37. Sastry, G.M.; Adzhigirey, M.; Day, T.; Annabhimoju, R.; Sherman, W. Protein and ligand preparation: Parameters, protocols, and influence on virtual screening enrichments. *J. Comput. Aided Mol. Des.* **2013**, *27*, 221–234. https://doi.org/10.1007/s10822-013-9644-8.
38. J. C. Shelley et al., "Epik: pKa prediction and protonation state generation," J. Comput. Aided Mol. Des., vol. 21, no. 12, pp. 681–691, 2007.
39. J. Kirchmair et al., "How to improve docking results: methods and metrics," J. Cheminform., vol. 7, S1, 2015, Art. O5.
40. A. N. Jain, "Surflex-Dock 2.1: development and benchmarking," J. Comput. Aided Mol. Des., vol. 21, no. 5, pp. 281–306, 2007.
41. J. C. Cole et al., "Gold: validation of a genetic algorithm for docking," Proteins, vol. 61, no. 2, pp. 243–256, 2005.
42. N. Homeyer and H. Gohlke, "Free energy of binding calculations with MM/GBSA," Mol. Inform., vol. 31, no. 2, pp. 114–122, 2012.
43. Genheden, S.; Ryde, U. The MM/PBSA and MM/GBSA methods to estimate ligand-binding affinities. *Expert Opin. Drug Discov.* **2015**, *10*, 449–461, https://doi.org/10.1517/17460441.2015.1032936.

 doi:10.20944/preprints202603.0799.v1

44. R. Salomon-Ferrer, A. W. Götz, D. Poole, S. Le Grand, and R. C. Walker, "Routine microsecond MD simulations with AMBER on GPUs," J. Chem. Theory Comput., vol. 9, no. 9, pp. 3878–3888, 2013.
45. Case, D.A.; Cheatham, T.E., III; Darden, T.; Gohlke, H.; Luo, R.; Merz, K.M., Jr.; Onufriev, A.; Simmerling, C.; Wang, B.; Woods, R.J. The Amber biomolecular simulation programs. *J. Comput. Chem.* **2005**, *26*, 1668–1688, doi:10.1002/jcc.20290.
46. V. J. Hearing and K. Tsukamoto, "Enzymatic control of melanogenesis," FASEB J., vol. 5, no. 14, pp. 2902–2909, 1991.
47. A. T. Slominski, M. A. Zmijewski, and R. Paus, "Melanin pigmentation system and melanoma biology," Physiol. Rev., vol. 94, no. 4, pp. 1159–1211, 2014.
48. A. Poli, R. Bianchi, and M. P. Visioli, "Squalene: chemistry, sources, and biological activities," Pharmacol. Res., vol. 44, no. 6, pp. 529–536, 2001.
49. C. Denkert et al., "Elevated COX-2 expression is linked to tumor progression and poor prognosis," Am. J. Pathol., vol. 162, no. 1, pp. 89–98, 2003.
50. J. Larkin et al., "Five-year survival with combined dabrafenib and trametinib in BRAF-mutated melanoma," N. Engl. J. Med., vol. 381, no. 7, pp. 626–636, 2019.
51. Kupcinskiene, E.; Stikliene, A.; Judzentiene, A. The essential oil qualitative and quantitative composition in the needles of Pinus sylvestris L. growing along industrial transects. *Environ. Pollut.* **2008**, *155*, 481–491, https://doi.org/10.1016/j.envpol.2008.02.001.
52. Nyamwihura, R.J.; Ogungbe, I.V. The pinene scaffold: its occurrence, chemistry, synthetic utility, and pharmacological importance. *RSC Adv.* **2022**, *12*, 11346–11375, https://doi.org/10.1039/d2ra00423b.
53. Salehi, B.; Upadhyay, S.; Erdogan Orhan, I.; Kumar Jugran, A.; L.D. Jayaweera, S.; A. Dias, D.; Sharopov, F.; Taheri, Y.; Martins, N.; Baghalpour, N.; C. Cho, W.; Sharifi-Rad, J. Therapeutic Potential of α- and β-Pinene: A Miracle Gift of Nature. Biomolecules 2019, 9, 738. https://doi.org/10.3390/biom9110738.
54. Trott, O.; Olson, A.J. AutoDock Vina: Improving the speed and accuracy of docking with a new scoring function, efficient optimization, and multithreading. *J. Comput. Chem.* **2010**, *31*, 455–461, https://doi.org/10.1002/jcc.21334.
55. Chapman, P.B.; Hauschild, A.; Robert, C.; Haanen, J.B.; Ascierto, P.; Larkin, J.; Dummer, R.; Garbe, C.; Testori, A.; Maio, M.; et al. Improved survival with vemurafenib in melanoma with BRAF V600E mutation. *N. Engl. J. Med.* **2011**, *364*, 2507–2516, doi:10.1056/nejmoa1103782.
56. Robert, C.; Karaszewska, B.; Schachter, J.; Rutkowski, P.; Mackiewicz, A.; Stroiakovski, D.; Lichinitser, M.; Dummer, R.; Grange, F.; Mortier, L.; et al. Improved overall survival in melanoma with combined dabrafenib and trametinib. *N. Engl. J. Med.* **2015**, *372*, 30–39, doi:10.1056/nejmoa1412690.
57. Nazarian, R.; Shi, H.; Wang, Q.; Kong, X.; Koya, R.C.; Lee, H.; Chen, Z.; Lee, M.-K.; Attar, N.; Sazegar, H.; et al. Melanomas acquire resistance to B-RAF(V600E) inhibition by RTK or N-RAS upregulation. *Nature* **2010**, *468*, 973–977, https://doi.org/10.1038/nature09626.
58. Arozarena, I.; Wellbrock, C. Overcoming resistance to BRAF inhibitors. *Ann. Transl. Med.* **2017**, *5*, 387–387, https://doi.org/10.21037/atm.2017.06.09.
59. Garutti, M.; Targato, G.; Buriolla, S.; Palmero, L.; Minisini, A.M.; Puglisi, F. CDK4/6 Inhibitors in Melanoma: A Comprehensive Review. *Cells* **2021**, *10*, 1334, https://doi.org/10.3390/cells10061334.
60. Levy, C.; Khaled, M.; Fisher, D.E. MITF: master regulator of melanocyte development and melanoma oncogene. *Trends Mol. Med.* **2006**, *12*, 406–414, https://doi.org/10.1016/j.molmed.2006.07.008.
61. Fabbro, D.; Cowan-Jacob, S.W.; Moebitz, H. Ten things you should know about protein kinases:IUPHAR Review 14. *Br. J. Pharmacol.* **2015**, *172*, 2675–2700, https://doi.org/10.1111/bph.13096.
62. Zhang, J.; Yang, P.L.; Gray, N.S. Targeting cancer with small molecule kinase inhibitors. *Nat. Rev. Cancer* **2009**, *9*, 28–39, https://doi.org/10.1038/nrc2559.
63. Kuźbicki, Ł.; Brożyna, A.A. Immunohistochemical detectability of cyclooxygenase-2 expression in cells of human melanocytic skin lesions: A methodological review. *J. Cutan. Pathol.* **2019**, *47*, 363–380, https://doi.org/10.1111/cup.13606.

 doi:10.20944/preprints202603.0799.v1

disclaim responsibility for any injury to people or property resulting from any ideas, methods, instructions or products referred to in the content.